Coupling Effects and Decoupling for Supersonic Flight Vehicle

Tain-Sou Tsay
Department of Department of Aeronautical Engineering
National Formosa University
64, Wen-Hua Road, Huwei, Yunlin
TAIWAN
tstsay@nfu.edu.tw

Abstract: -In this paper, a nonlinear decoupling technique is used to design an aerodynamic coupled missile flight control system. The decoupling are get from multiplications of two measurable accelerations and three controllable output commands of the autopilot. They give exact sign and magnitude of aerodynamic coupling directly in missile manoeuvre. From frequency responses of coupling terms, decoupling terms and inner open-loop Bode diagram of the rolling channel, it will be seen that the decoupling and robustness for aerodynamic couplings can be obtained simultaneously. The time responses give same conclusions.

Key-Words: - Aerodynamic Coupling, Decoupling, Missile Flight Control

1 Introduction

For high performance missile, simple rate feedback decoupling is not good enough to stabilize the considered system, especially for large angle of attacks. It is well known that large single-axis manoeuvre will result in serious unstable aerodynamic cross coupling for cruciform missile [l-12]. It will destabilize or degrade the performance of the system. Higher gain crossover frequency in the rolling channel and lower gain crossover frequencies in pitch/yaw channels are usually expected for against coupling from yawing/pitching channels. The concept of high gain of the rolling channel can viewed as a disturbance rejection design. However, it is limited by hardware, noisy environment, and system requirements; e.g., specifications of bandwidths of pitch/yaw channels for target engage. Another possible way is to use cross-decoupling controllers. In general, inverting the transfer function of plant is impossible for the considered system have large modeled, un-modeled uncertainties and large variations of cross-coupling terms. Proper reducing coupling effects is rather than exact eliminating. In this literature, multiplications of two measurable accelerations feedback signals of plant and three outputs of the autopilot are used to reduce coupling effects. They give exact sign and magnitude of aerodynamic coupling directly in missile manoeuvre. The decoupling behaviours are nonlinear. It will be linearized by small perturbation theorem for analyses and designs. The magnitudes of decoupling terms will be found by diagonalizing the state transition matrix of simplified roll-yaw coupled systems.

In the following sections, effects of aerodynamic couplings and feedback decoupling are discussed and evaluated by a simplified roll-yaw coupled system to find decoupling gains. From frequency responses of coupling terms, decoupling terms and inner open-loop Bode diagram of rolling channel, it will be seen that the decoupling and robustness against aerodynamic couplings can be obtained simultaneously. The time responses give same conclusions.

2 The Coupling Effects

The translational and rotational dynamics of the missile shown in Fig.1 are described by the following six nonlinear differential equations [1-3]:

$$\dot{U} = -\frac{\bar{q}s}{m}C_x - WQ + VR + \frac{F_{xg}}{m} \tag{1}$$

$$\dot{V} = -\frac{\bar{q}s}{m}C_y - UR + WP + \frac{F_{yg}}{m} \tag{2}$$

$$\dot{W} = -\frac{\bar{q}s}{m}C_z - VP + UQ + \frac{F_{zg}}{m} \tag{3}$$

$$\dot{P} = -\frac{l}{I_x}C_l \bar{q}sl \tag{4}$$

$$\dot{Q} = C_m \bar{q}sl - \frac{(I_x - I_z)}{I_y}PR \tag{5}$$

$$\dot{R} = C_n \bar{q}sl - \frac{(I_y - I_x)}{I_y}PQ \tag{6}$$

In above equations, U, V and W are velocity components measured on the missile body axes; P, Q and *R* are the components of the body angular rate: F_{xg}, F_{yg}, F_{zg} are the gravitational forces acting along the body axes: and I_x, I_y, I_z are the moments of inertia. The variable *s* is the reference area, $\bar{q}$ is the dynamic pressure

$$\bar{q} = \frac{1}{2}\rho(U^2 + V^2 + W^2) \equiv \frac{1}{2}\rho V_M^2 \tag{7}$$

l is the reference length. The aerodynamic lifting forces (C_x, C_y, C_z) and moments (C_l, C_m, C_n) are function of Mach number, angle of attack (α^*), angle of sideslip (β^*); the angles of attack and sideslip are defined as

$$\alpha^* = \tan^{-1}(\frac{W}{U}) \tag{8}$$

and

$$\beta^* = \tan^{-1}[(\frac{V}{V_M})/\cos\alpha^*] \tag{9}$$

The small signal perturbation model from a specified trim conditions(or operating point) (P^*, Q^*, R^*, $A_{ZO}, A_{YO}, \alpha^*, \beta^*$) of the considered system is described by following differential equations:

$$\dot{p} = L_p p + L_\alpha \alpha + L_\beta \beta + L_{\delta p}\delta p + L_{\delta q}\delta q + L_{\delta r}\delta r \tag{10}$$

$$\dot{q} = M_q q + M_\alpha \alpha + M_{\delta q}\delta q + M_{\delta p}\delta p \tag{11}$$

$$\dot{r} = N_r r + N_\beta \beta + N_{\delta r}\delta r + N_{\delta p}\delta p \tag{12}$$

$$\dot{\alpha} = -\tan\beta^* p + q + M_B(Z_\alpha \alpha + Z_{\delta q}\delta q + Z_{\delta p}\delta p) \tag{13}$$

$$\dot{\beta} = \tan\alpha^* p - r + M_B(Y_\beta \beta + Y_{\delta r}\delta r + Y_{\delta p}\delta p) \tag{14}$$

$$\begin{aligned} a_{zacc} = {} & Z_\alpha \alpha + Z_{\delta q}\delta q + Z_{\delta p}\delta p - l_S(M_q q \\ & + M_\alpha \alpha + M_{\delta p}\delta p + M_{\delta q}\delta q) \end{aligned} \tag{15}$$

$$\begin{aligned} a_{yacc} = {} & Y_\beta \beta + Y_{\delta r}\delta r + Y_{\delta p}\delta p + l_S(N_r r \\ & + N_\beta \beta + N_{\delta p}\delta p + N_{\delta r}\delta r) \end{aligned} \tag{16}$$

where *p, q, r* are body angular rate deviations from trims (P^*, Q^*, R^*); a_{zacc}, a_{yacc} are body acceleration deviations from trims (A_z^*, A_y^*); and α and β are the angles of attack and sideslip deviations from trims (α^*, β^*), l_S is the distance between sensor position and Central of Gravity(CG). $L_{(\bullet)}, M_{(\bullet)}, N_{(\bullet)}, Y_{(\bullet)}$ and $Z_{(\bullet)}$ represent derivatives of moments (C_l, C_m, C_n)/ forces (C_y, C_z) with respect to *p, q, r,* $\alpha, \beta, \delta p, \delta q, \delta r$.

For skid-to-turn missile, only yawing/pitching channels to rolling channel will be considered for the rolling command δp is always zero. For large angle of attack(α^*) and small sideslip angle(β^*), the magnitude of terms $\tan\beta^*$ and L_α are much less than those of $\tan\alpha^*$ and L_β, thus the original 3×3 system can be decomposed into a 2×2 roll-yaw coupled system and pitching system. Similar to the case of large β^* and small α^*, it can be decomposed into a 2×2 roll-pitch coupled system and a yawing system. For simplicity and illustration, only the 2×2 roll-yaw coupled system will be discussed in this literature. The state space model of the rolling/yawing coupled system is

$$\begin{bmatrix} \dot{p} \\ \dot{r} \\ \dot{\beta} \end{bmatrix} = \begin{bmatrix} L_p & 0 & L_\beta \\ 0 & N_r & N_\beta \\ \tan\alpha^* & -1 + MBY_r & MBY_\beta \end{bmatrix} \begin{bmatrix} p \\ r \\ \beta \end{bmatrix} + \begin{bmatrix} L_{\delta p} & L_{\delta r} \\ N_{\delta p} & N_{\delta r} \\ 0 & MBY_{\delta r} \end{bmatrix} \begin{bmatrix} \delta p \\ \delta r \end{bmatrix} \tag{17}$$

$$\begin{aligned} \begin{bmatrix} a_{ycg} \\ a_{yacc} \end{bmatrix} = {} & \begin{bmatrix} 0 & 0 & Y_\beta \\ 0 & Y_r + l_S N_r & Y_\beta + l_S N_\beta \end{bmatrix} \begin{bmatrix} p \\ r \\ \beta \end{bmatrix} \\ & + \begin{bmatrix} Y_{\delta p} & Y_{\delta r} \\ Y_{\delta p} + l_S N_{\delta p} & Y_{\delta r} + l_S N_\beta \end{bmatrix} \begin{bmatrix} \delta p \\ \delta r \end{bmatrix} \end{aligned} \tag{18}$$

where a_{ycg} is the acceleration at central gravity of mass, and a_{yacc} is the measured acceleration at the location of sensor. It is most desired to reduce the effect of L_β shown in Equation (17) or diagonalizing upper triangular of the state transition matrix of the state-space model given in Equation (17). Now, consider the major coupling effects from yawing channel to rolling channel to be decoupled, the transfer function of $p/\delta r$ becomes:

$$\frac{p}{\delta r}=\frac{L_{\delta r}s^2+[L_\beta Y_{\delta r}MB-L_{dr}(N_r+MBY_\beta)]s-L_\beta(N_{\delta r}+Y_{\delta r}MBN_r)+L_{\delta r}(N_\beta+N_rMBY_\beta)}{s^3-(L_p+N_r+MBY_\beta)s^2+(L_pN_r+N_\beta+L_pMBY_\beta+N_rMBY_\beta-\tan\alpha^*L_\beta)s-L_p(N_\beta+N_rMBY_\alpha)+N_r\tan\alpha^*L_\beta} \quad (19)$$

The denominator of Equation (19) can be approximated by

$$\Delta(s)=s^3-(L_p+N_r+MBY_\beta)s^2+(N_\beta-a^*L_\beta)s-L_pN_\beta+N_r\alpha^*L_\beta \quad (20)$$

for

$\tan\alpha^*\cong a^*$;

$|N_\beta-\alpha^*L_\beta|>>|L_pN_r+L_pMBY_\beta|$;

$|-L_pN_\beta+N_r\alpha^*L_\beta|>>|L_pN_rMBY_\beta|$

Since the value of N_r is negative for stable static margin, the positive value of α^*L_β is called the unstable aerodynamic coupling for it will destabilize or degrade performance of the system; negative value of α^*L_β is called the stable aerodynamic coupling. Similar to $p/\delta r$, one find that the positive value of β^*L_α from $p/\delta q$ is called the stable aerodynamic coupling; negative of β^*L_α is called the unstable aerodynamic coupling. Thus the characteristic of the system is largely affected by the coupling term β^*L_α(or α^*L_β). α^*L_β(or β^*L_α). Note that one may pay more attention for unstable aerodynamic coupling while leaving stable aerodynamic coupling alone. Large value of α^* /small value of β^* are corresponding to large value of A_{ZO} / small value of A_{YO}. Those imply that coupling terms to rolling channel are function of longitudinal/ lateral maneuvers (A_{ZO}, A_{YO}). In the following section, a special decoupling block will be applied to introduce decoupling term including α^*L_β and β^*L_α.

3. The Decoupling Algorithm

The major coupling terms stated above are α^*L_β and β^*L_α. The problem of decoupling algorithm is to find measurable/controllable datum proportional to those of α^*L_β and β^*L_α. There are five measurable datum (A_{YF}, A_{ZF}, P_f, Q_f, R_f) and three controllable variables ($\delta pc, \delta qc, \delta rc$) shown in Fig.2 can be used for decoupling[12-13]. Consider a nonlinear decoupling configuration shown in Fig.2. The mathematical representation of decoupling block is

$$\Delta_p^{'}=\Delta_p+K_1A_{ZF}\times\Delta_r+K_2A_{YF}\times\Delta_q \quad (21)$$

$$\Delta_q^{'}=\Delta_q+K_3A_{YF}\times\Delta_p \quad (22)$$

$$\Delta_r^{'}=\Delta_r+K_4A_{ZF}\times\Delta_p \quad (23)$$

where $\Delta_{(\bullet)}$ terms are output commands of autopilot without decoupling , $\Delta'_{(\bullet)}$ terms are output commands with decoupling, and K_1, K_2, K_3, and K_4 are gains of decoupling loop to be applied. Similar derivations of Equations (10) to (16), the small signal linear perturbation equations of Equations (21) to (23) from trim conditions (A_{ZO}, A_{YO}, $\delta qo, \delta ro$) are

$$\delta p'=\delta p+K_1(A_{ZO}\delta r+a_{zacc}\delta ro)+K_2(A_{YO}\delta q+a_{yacc}\delta qo) \quad (24)$$

$$\delta q'=\delta q+K_3A_{YO}\delta p \quad (25)$$

$$\delta r'=\delta r+K_4A_{ZO}\delta p \quad (26)$$

with $\Delta_p=\delta po+\delta p;\Delta_q=\delta qo+\delta q;\Delta_r=\delta ro+\delta r;$ $A_{YF}=A_{YO}+a_{yacc};A_{ZF}=A_{ZO}+a_{zacc}$ and $\delta po\equiv 0$ for skid to turn missile. Signal flows with Equations(24) to (26) are given in Fig.3. Note that ($\delta p, \delta q, \delta r$) are replacing($\delta pc, \delta qc, \delta rc$), those are outputs of de-mixer of four actuators cascaded to($\delta_{1c}, \delta_{2c}, \delta_{3c}, \delta_{4c}$) shown in Fig.3. It shows the linearized control configuration for analysis and design. Equation (24) includes $A_{ZO}\delta r$ and $A_{YO}\delta q$. It implies that proper values of K_1 and K_2 will decouple the coupling terms α^*L_β and β^*L_α. Equations (24) to (26) can be further simplified as given below:

$$\delta p'=\delta p+K_1A_{ZO}\delta r+K_2a_{yacc}\delta qo \quad (27)$$

$$\delta r'=\delta r+K_4A_{ZO}\delta p \quad (28)$$

for large angle of attack(α^*) with small angle of sideslip(β^*). For simplicity and illustration,

hardware and compensations are first neglected to derive close form solutions of K_1, K_2, K_4. Since the gain crossover frequencies of inner loops are usually greater than those of outer loops, outer loop shown in Fig.3 can be neglected for decoupling analyses. Frequency and time responses will verify this simplification. The inputs of plant of inner loops closed-loop system can be written as follows:

$$\delta p' = -K_{ip} p + K_1 A_{ZO} \delta r + K_2 a_{yacc} \delta qo \quad (29)$$

$$\delta r' = K_{ir} r + K_4 A_{ZO} \delta p \quad (30)$$

and after $(\delta p, \delta r)$ given in Equation (17) replace by $(\delta p', \delta r')$ given in Equations (29) and (30), the state-space model of this closed-loop system with decoupling becomes

$$\begin{bmatrix} \dot{p} \\ \dot{r} \\ \dot{\beta} \end{bmatrix} = \begin{bmatrix} a_{11} & a_{12} & a_{13} \\ a_{21} & a_{22} & a_{23} \\ a_{31} & a_{32} & a_{33} \end{bmatrix} \begin{bmatrix} p \\ r \\ \beta \end{bmatrix} \quad (31)$$

The decoupling can easily be achieved by setting off-diagonal elements of Equation (31) to be zeros. Since the considered system is a skid-to-turn missile, the major terms of Equation(31) for decoupling are from yawing channel to rolling channel are a_{13},a_{12} and from rolling channel to yaw channel are a_{21}. Three elements (a_{13},a_{12}, a_{21}) are selected for three gains (K_1, K_2, K_4) are needed. They are in the form of

$$a_{12} = HK_{ir} L_{\delta r} + L_{\delta p} \{K_2 \delta qo N_r + K_{ir} [K_2 \delta qo (Y_{\delta r} + l_S N_{\delta r}) + K_1 A_{ZO}]\} \quad (32)$$

$$a_{13} = L_\beta + HK_2 \delta qo L_{\delta p} (Y_\beta + l_S N_\beta) \quad (33)$$

$$a_{21} = -K_{ip} HN_{\delta p} \{1 + K_4 A_{ZO} [K_1 A_{ZO} + K_2 \delta qo (Y_{\delta r} + l_S N_{\delta r})]\} - K_{ip} K_4 N_{\delta r} A_{ZO} \quad (34)$$

where $H = [1 - K_2 \delta qo (Y_{\delta p} + l_S N_{\delta p})]^{-1}$. Let a_{13}, a_{12} and a_{21} be zeros for aerodynamic coupling and find solutions of K_1, K_2, K_4. They are in the form of

$$K_2 = \frac{-L_\beta}{\delta qo [L_{\delta p} (Y_\beta + l_S N_\beta) - L_\beta (Y_{\delta p} + l_S N_{\delta p})}} \quad (35)$$

$$K_1 = \frac{K_2 \{HL_{\delta p} \delta qo [l_S N_r + K_{ir} (Y_{\delta r} + l_S N_{\delta r})]\} + K_{ir} L_{\delta r}}{HL_{\delta p} K_{ir} A_{ZO}} \quad (36)$$

$$K_4 = \frac{HN_{\delta p}}{N_{\delta r} A_{ZO} + HN_{\delta p} A_{ZO} [K_1 A_{ZO} + K_2 (Y_{\delta r} + l_S N_{\delta r})]} \quad (37)$$

Equations (35) to (37) give K_1, K_2, K_4 are function of K_{ir} only. Since there are modeled and un-modeled uncertainties for aerodynamic coefficients given in Equations (10) to (16), the values of K_1, K_2, K_4 selected for reducing the coupling effects rather than exact cancellation. Naturally, the effects of decoupling will be degraded with hardware added. Thus the effects of hardware may need to be considered to choice proper gains of decoupling loop or to compensate the system which distorted by hardware. Since the responses of $\delta p, \delta r$ are dependent on the gain crossover frequencies of rolling/yawing inner loop, thus if gain crossover frequencies were unaffected by introducing hardware, the found decoupling are unaffected.

4. The Analyses Results

The small perturbation aerodynamic coefficients of the considered system are given in Appendix A[15,16] for variable angle of attacks(α^*) and sideslip (β^*). It gives that performance and robustness of the considered system will be affected by L_β for maximal value of coupling coefficient L_β is two third of $L_{\delta p}$. In general, three SISO systems; i.e., rolling/pitching/yawing channels, are designed first, and then connected them with aerodynamic / kinematical coupling term; i.e., MIMO system for verification the suitability of SISO designs. Several iterations are usually needed. Table 1 gives SISO design and MIMO analyzed results. The gains(K_{op}, K_{ip}, K_{oq}, W_{iq}, K_{or}, W_{ir}, K_{ir}) are give in Appendix A with a gain adjusting logic for K_{ip} and K_{op}:

$$Sckip = 0.025 |A_{ZO}| + 1.4; K_{ip} = Sckip \times K_{ipo};$$

$$Sckop = 0.030 | A_{ZO} | +1.4; K_{op} = Sckop \times K_{opo};$$

The used of *Sckip* and *Sckop* is to against aerodynamic couplings for large angle of attacks. They are functions of A_{ZO}. The compensations and hardware dynamics are given in Appendix B also. From Table 1, one can see that it is a good designs for good robustness (GM $\geqq$ 6dBs, PM$\geqq$60degs); and low-frequency gain margins (LFGM) are reduced incrementally for larger coupling term added. The effects of coupling terms for (α^*, β^*) = (12°, 1°) are shown in Fig.4 for only rolling inner loop open. The solid-lines are frequency responses of the rolling channel SISO system. The doted-lines are frequency responses MIMO system; i.e.; 2×2 roll-yaw coupled system. Fig.4 shows that loop gain are largely reduced by introducing coupling terms. The corresponding LFGM, High-frequency-Gain-Margin (HFGM) and Phase Margin (PM) are given in Table 1. Table 1 gives that LFGMs are unacceptable for α^*>6°. The system is nearly unstable for $\alpha^* \geq 12°$.

Table 2 gives the analyzed results with decoupling terms added. K_1, K_2, K_4 are found by Equations (35) to (37). It gives LFGMs become acceptable (LFGM $\leqq$ 0.53), and PMs approach 60degs. The effective of decoupling is shown in Fig.4(dashed-line). It recovers the magnitude form coupled system (doted-line). Note that the effective for decoupling of two-axis maneuvering (α^*, β^*) = (10°, 8°) are given in Tables 1 and 2 also. Note also that K_1, K_2, K_4 are found from simplified system without compensation and hardware added. The effects of compensation and hardware must be analyzed for suitability of the proposed decoupling block and K_1, K_2, K_4. Fig.5 shows the variation for four combination conditions with/without decoupling and with/without compensation and hardware. Fig.5 shows the responses of coupling responses p / A_{YC} for (α^*, β^*) = (12°, 1°). The doted-line shows the responses without decoupling/ without hardware and compensations; the dash-doted-line shows responses with decoupling/without hardware and compensations; the solid-line shows responses without decoupling/ with hardware and compensation; the dashed-line shows responses with decoupling/with hardware and compensation. From Fig.4. it can be seen that the decoupling almost not affected by hardware and compensation added or not. It implies also that the evaluation for K_1, K_2, K_4 with diagonalizing the state transition matrix of the simplified give effective way for finding decoupling. Fig. 6 shows frequency responses p / A_{YC} for α^* varying from 1° to 12°. It gives the maximal value of rolling rate is less than 5 deg/sec for β^*=1°. All analyzed results stated above will be verified by time responses with the control configuration shown in Fig.3.

5. Simulation Verifications

Figs.7 shows the 5-DOF simulating results for (A_{ZC}, A_{YC}) = (-22.3G, -1.42G) without decoupling loops. The control configuration shown by Fig.3 excluding the proposed decoupling block is used in 5-DOF simulation. Output limitations for ($\delta pc, \delta qc, \delta rc$) are (±5°,±20°,±20°). This operating condition is corresponding to trim condition (α^*, β^*) = (12°, 1°). Fig.7 shows the compensated system is nearly unstable for sustaining oscillating of A_{ZF}, P_F, R_F *and* β. The oscillating frequency is 2.75Hz. Fig.6 gives same conclusion in frequency domain.

Fig.8 shows simulating results with decoupling described by Equation (21) to (23). It can be seen that the performance and stability of the system are improved significantly. The maximal value of rolling angular rate is equal to -15.6 deg/s. Note that constant decoupling gains given in Table 2 for (α^*, β^*) = (12°, 1°) are used in whole simulation. ± 5G varying testing for A_{ZC} are applied after 2 seconds. It is corresponding to angle of attack (α^*) varying from 10° to 14°. These testing give decoupled behavior keeps almost unchanged for plant variations (emulating system uncertainties). Fig.9 shows simulation results for (α^*, β^*) = (1°, 1°) with decoupling gains found for (α^*, β^*) = (12°, 1°). It can be seen that over decoupling is avoided for small values of (A_{ZF}, A_{YF}) are used in decoupling loops.

6. Conclusions

In this paper, decoupling gains are found by diagonalizing state transition matrix and effects of decoupling loop are discussed in frequency domain. The gains of decoupling loop can be found easily by simplified system and verified by adding hardware. The decoupling loop gives possible way to against

aerodynamic coupling for high performance missile and can be formulated easily as functions of velocity, altitude, and angle of attack for digital flight control system.

References:

[1] D.V. Stallard, Decoupling the Flight Control System of a Cruciform Missile, AIAA- Paper-76-1943, pp.236-246, 1976.

[2] A. Arrow and D.J. Yost, Large Angle of Attack Missile Control Concepts for Aerodynamic Controlled Missiles, J. of Spacecraft, Vol.14, No.10, pp.606-613 , 1977.

[3]C.A. Desoer and A.N. Gunds, Decoupling Linear Multiinput Multioutput Plant by Dynamic Output Feedback: an algebraic theory, IEEE Trans. on Automatic Control, Vo1.31, pp.744-750, 1986.

[4] C.Snell, S.A., Englewood, D. F. Enns and W. L. Garrard, Nonlinear Inversion Flight Control for a Supermaneuver Aircraft, Journal of Guidance, Control and Dynamics Vo1.15, No.4, pp.976-984, 1992.

[5] S.H. Lane and R.F. Stengel, Flight Control Design Using Nonlinear Inverse Dynamics, Automatica, Vol. 24, pp.471-484, 1988.

[6] D.D. Enns, R. Bugajski and G. Stein, Dynamic Inversion: an Evolving Methodology for Flight Control Design, Int. J. of Control, Vol.59, pp.71-91, 1994.

[7] S.A. Snell and. P. W Stout, Flight Control Law Using Nonlinear Dynamic Inversion Combined With Quantitative Feedback Theory, Journal of Dynamic Systems, Measurement and Control, Vol.120, No.2, pp.208-214, 1998.

[8] W. Siwakosit, S.A. Snell and, R.A. Hess, Robust Flight Control Design with Handling Qualities Constraints using Scheduled Linear Dynamic Inversion and Loop-Shaping, IEEE Trans. on Control Systems Technology, Vol.8, No.3, pp.483-494, 2000.

[9] J. Reiner, G.J. Balas and W. J. Garrard, Flight Control Design Using Robust Dynamic Inversion and Time-scale Separation, Automatica, Vol.32, No.11, pp. 1493-1504, 1996.

[10] R.J. Adams and S.S. Banda, Robust Flight Control Design Using Dynamic Inversion and Structured Singular Value Synthesis, IEEE Trans. on Control System Technology, Vo1.2, No.2, pp.80-92, 1993.

[11]J.H. Blakelack, Automatic Control of Aircraft and Missile, Second Edition, John Wiley and Sons, New York, 1991.

[12]T. S. Tsay, Decoupling the Flight Control System of a Supersonic Vehicle, Aerospace Science and Technology, Vol.11, No.7-8, pp.553-562, 2007.

[13]F.W. Nesline and P. Zarchan, Robust Instrumentation Configurations for Homing Missile Flight Control," AIAA Guidance Control Conference, AIAA-Paper- 80- 1749, pp.209-219, 1980.

[14]F.W. Nesline and M.L. Nesline, How Autopilot Requirements Constraint the Aerodynamic Design of Homing Missile, American Control Conference, pp.716-730, 1984.

[15]W.J. Monta, Supersonic Aerodynamic Characteristics of An Air-to-air Missile Configuration with Cruciform Wings and In-line Tail Control, NASA-TM-X- 2666, Langley Research Center, Hampton, Virginia, 1972.

[16]W.J. Monta, Supersonic Aerodynamic Characteristic of A Sparrow III Type Missile Model With Wing Control and Comparison with Existing Tail-control Results, NASA- TR-1078, Langley Research Center, Hampton, Virginia, 1977.

Appendix A: Aerodynamic Coefficients and Loop Gains

Seven sets of aerodynamic coefficients and trim values A_{ZO}, A_{YO}, $\delta qo, \delta ro$ of an air-to-air missile (AAM) at VM=676.8m/s are given below:

	$L_{\delta q}$ =780.45,	$L_{\delta p}$ =14609.0,	$L_{\delta r}$ =780.45,	$\boldsymbol{L_p}$ = -4.798,	M_q =-3.232,
	N_r =-3.232,	N_β =274.03,	$N_{\delta r}$ =-599.7,	$N_{\delta p}$ =-29.99,	$Z_{\delta q}$ =-30.61,
	Y_β =-95.85,	$M_{\delta q}$ =-599.7,	$M_{\delta p}$ =-29.99,	$Y_{\delta r}$ =30.611,	$Y_{\delta p}$ = 0.000,
	K_{opo} =15.58	K_{ipo} =0.0031	K_{oq} =0.0744	W_{iq} =15.98	K_{iq} =0.0409
	l_S =0.147	M_B =0.0145	K_{or} =0.0744	W_{ir} =15.98	K_{ir} =0.0409
A1.	α^* =12.00°,	β^* =1.00°,	L_α =684.45,	L_β = 8951.6,	Z_α =-176.65,
	M_α =-739.53,	δro =0.46°,	δqo =-11.33°,	A_{YO} =-1.42G,	A_{ZO} =-22.3G,
A2.	α^* =10.00°,	β^* =1.00°,	L_α =809.8,	L_β =7324.1,	Z_α =-171.4
	M_α =-714.14	δro =0.46°,	δqo =-8.86°,	A_{YO} =-1.42G	A_{ZO} =-17.53
A3.	α^* =8.00°,	β^* =1.00°,	L_α =623.76,	L_β = 5787.7,	Z_α =-161.45,
	M_α =-635.83,	δ_r^* =0.46°,	δqo =-6.17°,	A_{YO} =-1.42G,	A_{ZO} =-13.1G,
A4.	α^* =6.00°,	β^* =1.00°,	L_α =518.8,	L_β = 4446.8,	Z_α =-136.9,
	M_α =-490.96,	δro = 0.46°,	δqo =-3.83°,	A_{YO} = -1.42G,	A_{ZO} =-9.11G,
A5.	α^* =4.00°,	β^* =1.00°,	L_α =606.29,	L_β = 2835.8	Z_α =-109.16,
	M_α =-351.55,	δro = 0.46°,	δqo =-2.12°,	A_{YO} = -1.42G,	A_{ZO} =-5.77G,
A6.	α^* =4.00°,	β^* =1.00°,	L_α =1510.1,	L_β =-528.8,	Z_α =-97.29
	M_α =-286.1	δro =0.46°,	δqo =-2.13°,	A_{YO} =-1.42G	A_{ZO} =-2.83G
A7.	α^* =1.00°,	β^* =1.00°,	L_α =2789.6	L_β = -2789.6	Z_α =-95.85,
	M_α =-274.03,	δro = 0.46°,	δqo =-0.46°,	A_{YO} = -1.42G,	A_{ZO} =-1.42G,

Appendix B: Compensators and Hardware Models

1. Rolling outer/inner loop compensators cascaded to K_{op}/K_{ip}

$$POC(Z)=\frac{0.7500Z-0.5100}{Z-0.7600}$$

$$PIC(Z)=\frac{1.0063Z-0.9917}{Z-0.9980}\times\frac{2.3358Z^3-3.2585Z^2+1.9410Z-0.4413}{Z^3-0.6889Z^2+0.3109Z-0.0449}$$

2. Yawing outer/inner loop compensator cascaded to $K_{or}/W_{ir}/K_{ir}$

$$OC(Z)=\frac{1.3087-1.0091}{Z-0.7005}$$

$$SC(Z)=0.0025\frac{Z+1}{Z-1}$$

$$IC(Z)=\frac{1.7091-0.7091}{Z}$$

3. Actuator models

$$CAS(S)=\frac{98696}{S^2+188.5S+98696}$$

4. Rate gyro/accelerometer models

$$RG(S)=\frac{193444}{S^2+263.9S+193444}$$

5. Inner loop low-pass filter body angular rate

$$LPFI(S)=\frac{314.2}{S+314.2}$$

6. Outer loop low-pass filter for acceleration

$$LPFO(S)=\frac{188.5}{S+188.5}$$

Table 1. SISO System and MIMO System without Decouple

	SISO System		MIMO without Decouple		
α^*/β^*	HFGM	PM	LFGM	HFGM	PM
12°/1°	1.85	60.3°	0.97	1.89	8.39°
10°/1°	1.97	62.3°	0.76	2.00	64.7°
8°/1°	2.10	64.2°	0.57	2.12	65.8°
6°/1°	2.23	65.8°	0.39	2.24	66.9°
4°/1°	2.35	67.2°	0.21	2.35	67.8°
2°/1°	2.47	68.3°	----	2.46	68.6°
1°/1°	2.53	68.9°	----	2.52	69.2°
10°/8°	1.97	61.7°	0.50	1.99	64.0°

Table 2. MIMO System with Decouple Loops

	MIMO with Decouple Loops					
α^*/β^*	LFGM	HFGM	PM	K_1	K_2	K_4
12°/1°	0.53	1.68	53.8°	-0.0522	-0.0731	0.0035
10°/1°	0.46	1.81	58.1°	-0.0519	-0.0746	0.0046
8°/1°	0.39	1.94	61.6°	-0.0521	-0.0827	0.0063
6°/1°	0.30	2.08	64.5°	-0.0540	-0.1006	0.0093
4°/1°	0.19	2.24	66.8°	-0.0473	-0.1129	0.0150
2°/1°	----	2.54	68.2°	0.0543	+0.0454	0.0321
1°/1°	----	2.68	68.2°	0.2958	+0.4807	0.0664
10°/8°	0.37	1.85	59.5°	-0.0353	-0.0528	0.0048

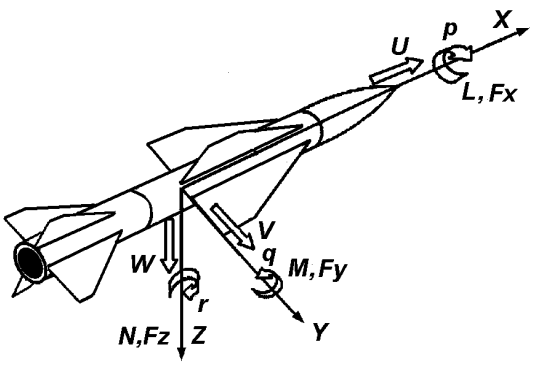

Fig.1. Coordinated System Definitions.

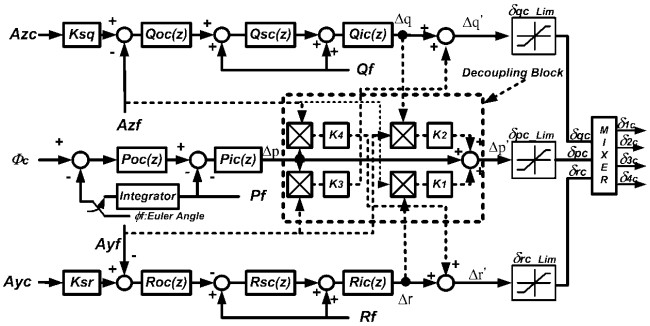

Fig.2. Digital Autopilot with Nonlinear Feedback Decoupling Block.

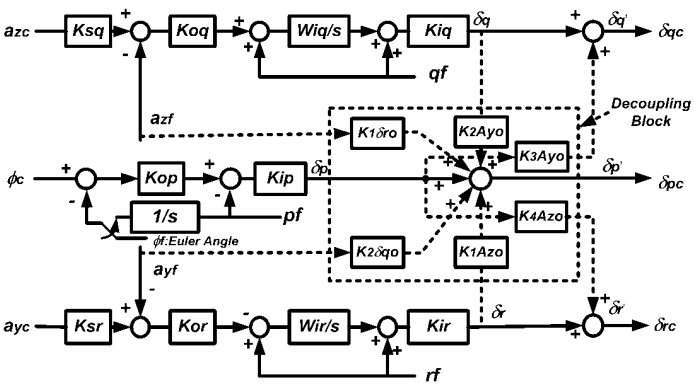

Fig.3. Linearized Control Configuration for Analyses.

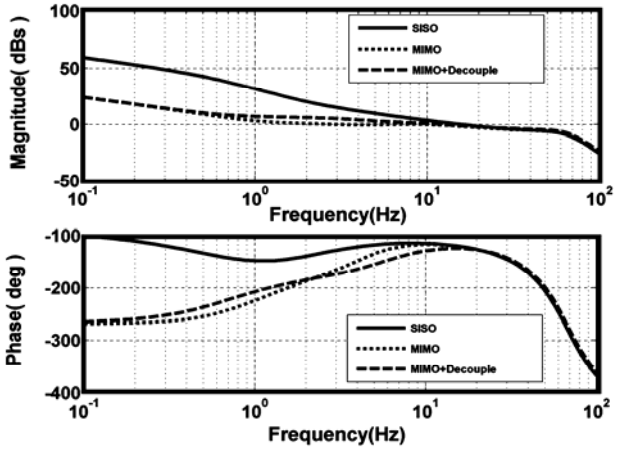

Fig.4. Open-loop Bode Diagrams of Rolling Channel.

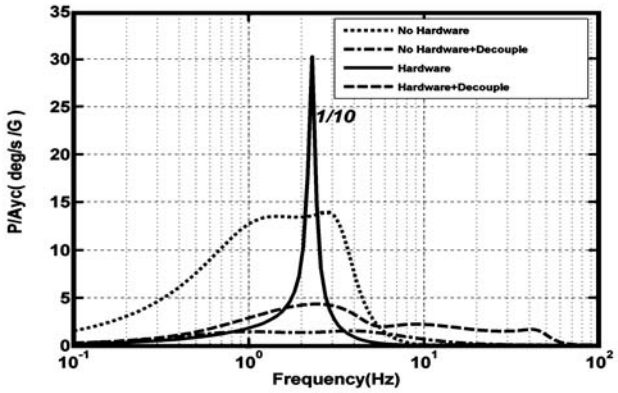

Fig.5. Frequency Responses of p/Ayc for (α^*, β^*)=(12°,1°).

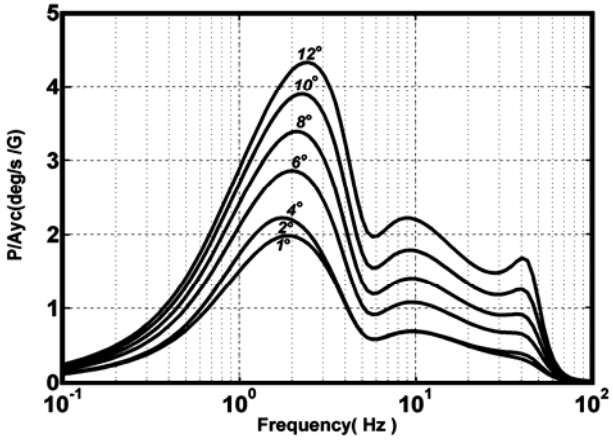

Fig.6. Frequency Responses of p/Ayc for α^* varying .

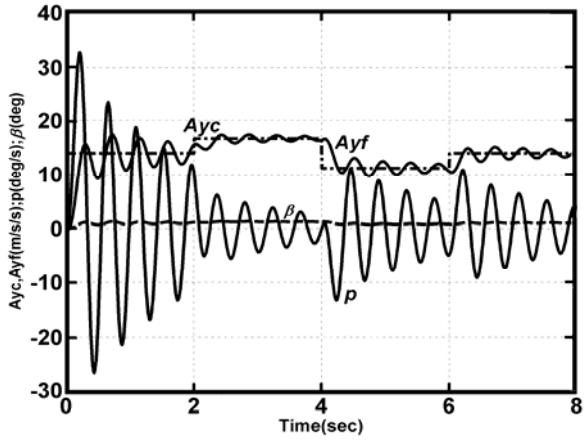

Fig.7. Time Responses for (α^*, β^*)=(12°,1°) without Decoupling Loop.

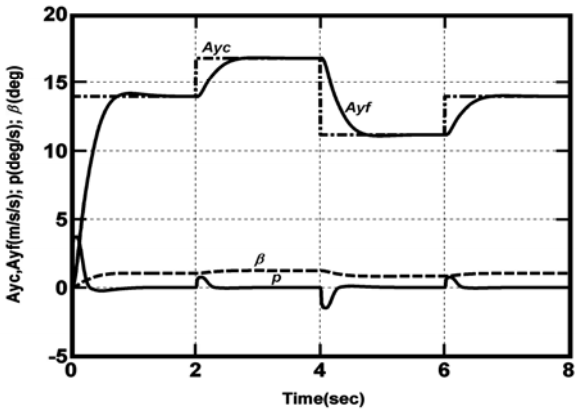

Fig.8. Time Responses for (α^*, β^*)=(12°,1°). with Decoupling Loop.